

## Recent trends and open questions in grain boundary segregation

Pavel Lejček<sup>a)</sup>

*Institute of Physics, Academy of Sciences of the Czech Republic, 182 21 Praha 8, Czech Republic*

Monika Všíanská and Mojmír Šob

*Central European Institute of Technology, Masaryk University, CEITEC MU, 625 00 Brno, Czech Republic; Institute of Physics of Materials, Academy of Sciences of the Czech Republic, 616 62 Brno, Czech Republic; and Department of Chemistry, Faculty of Science, Masaryk University, 611 37 Brno, Czech Republic*

(Received 19 April 2018; accepted 21 June 2018)

Recently, significant progress in the field of grain boundary segregation was achieved, for example, in better understanding and modeling the stabilization of nanocrystalline structures by grain boundary segregation, searching for more advanced approaches to theoretical calculation of segregation energies and development of the complexion approach. Nevertheless, with each progress, new important questions appear which need to be solved. Here, we focus on two basic questions appearing recently: How can be the experimental results on the grain boundary segregation compared reliably to their theoretical counterparts? Is the preferred segregation site of a solute in the grain boundary core substitutional or interstitial? We also show that the entropy of grain boundary segregation is a very important quantity which cannot be neglected in thermodynamic considerations as it plays a crucial role, for example, in prediction of thermodynamic characteristics of grain boundary segregation and in the preference of the segregation site at the boundary.

### I. INTRODUCTION

The phenomenon “grain boundary segregation” is known for decades. Although the first indirect evidence of the effect of changed composition of grain boundaries of copper on interfacial cohesion has been reported already in 19th century,<sup>1</sup> probably the first direct reference in the literature comes from 1950s when Stewart et al.<sup>2</sup> showed by autoradiography that polonium (i.e., radioactive isotope <sup>210</sup>Bi) enriches grain boundaries in lead. After the starting period of indirect detection, extended studies of grain boundary segregation have been facilitated by the development of surface analytical techniques such as Auger electron spectroscopy (AES), X-ray photoelectron spectroscopy (XPS or ESCA—electron spectroscopy for chemical analysis), etc.<sup>3</sup> In this respect, the publication of Kalderon explaining the reasons for catastrophic damage of the rotor in the Hinkley Point power station in 1968 represents the very first application of AES in the field of grain boundary segregation.<sup>4</sup> Since that time, numerous studies of grain boundary segregation of various solutes in different host metals were published. Somewhat later, molecular dynamics (MD)<sup>5</sup> and tight binding (TB)<sup>6</sup> calculations of the energy of grain boundary segregation have been

started. Besides them, various other approaches to theoretical calculations have been later developed, mainly Monte Carlo and density functional theory (DFT) as summarized in the recent review.<sup>7</sup>

During those more than 70 years of real and intensive study of the grain boundary segregation, extensive understanding of this phenomenon was achieved. The development of this field can be documented, e.g., by establishment of its thermodynamics and kinetics, development of models for description of chemical composition of the interfaces in real multicomponent systems, models of nonequilibrium segregation joined mainly with material irradiation or deformation, and the relationship of the segregation with metallurgical problems such as intergranular embrittlement and grain boundary engineering (GBE).<sup>8</sup> In the following, we will present recent trends and achievements and discuss some open questions appearing during the development of the field.

### II. RECENT TRENDS IN STUDYING GRAIN BOUNDARY SEGREGATION

The recent studies of grain boundary segregation have been focused on the following tasks: (i) stabilization of grain size (i.e., nanocrystalline structures) by grain boundary segregation; (ii) relationship between grain boundary segregation and changes of intercrystalline cohesion; (iii) GBE; and (iv) nonequilibrium segregation. Extensive attention has also been paid to (v) development

<sup>a)</sup>Address all correspondence to this author.

e-mail: lejcekp@fzu.cz

This paper has been selected as an Invited Feature Paper.

DOI: 10.1557/jmr.2018.230

of new techniques to experimental studies of grain boundary segregation; (vi) theoretical calculations of the segregation energy including development of new procedures of these calculations; and (vii) studies of grain boundary segregation in nonmetallic systems. Besides, (viii) new models of grain boundary segregation have been proposed including considerations of the segregation site in the grain boundary core; and (ix) development of the concept of grain boundary complexions which also shows the importance of the segregation entropy as a decisive parameter describing this phenomenon. During the last 5 years, more than 500 papers related to these 9 basic trends were published according to the Scopus database, which documents that the interest in the field of grain boundary segregation is permanently stable and large. Let us briefly summarize the recent effort in the individual issues listed above.

Stabilization of grain boundaries by grain boundary segregation has been frequently studied with extended interest as the importance of nanocrystalline materials is growing similarly as the requirements on their stability at enhanced temperatures. Solute segregation is one of the main stabilizing features and has been investigated from various viewpoints and model formulations.<sup>9–14</sup> In this respect, the effect of entropy is also often considered as its importance increases with increasing temperature.<sup>15</sup> The present task is to find the rules for stabilizing effects and selection of suitable systems in which the nanocrystalline structure remains unchanged. In this respect, positive enthalpy of mixing plays the crucial role.<sup>9–11</sup> The effect of the grain boundary segregation on the stabilization of nanocrystalline structures consists in complex link of reduced grain boundary energy, boundary migration kinetics, and mobility<sup>13</sup> which is often anisotropic: in such case, growth of few grains is thus possible on account of the otherwise stabilized nanostructure.<sup>16</sup> This is inevitable, however, as few but large grains may appear in the materials similarly to the abnormal grain growth. Typical hosts for the study of the grain size stabilization are nickel,<sup>14,15,17</sup> tungsten,<sup>18</sup> and iron.<sup>14</sup> Great attention is also paid to immiscible nanocrystalline alloys.<sup>19</sup> Indeed, the solute segregation is not the single stabilizing effect of the nanostructure: Another one is the drag of the boundary migration caused by presence of precipitates (e.g., Zener drag). However, the necessary condition for formation of the precipitates at the grain boundaries is preceding solute segregation at those regions.<sup>20</sup>

Another consequence of grain boundary segregation is segregation-induced change of intergranular cohesion. This subject is mainly studied on technologically important and/or prospective materials as nickel,<sup>7,21–23</sup> tungsten,<sup>24,25</sup> iron,<sup>7,26–28</sup> aluminum,<sup>29–31</sup> magnesium,<sup>32</sup> vanadium,<sup>33</sup> niobium,<sup>34</sup> and NiAl.<sup>35</sup> The quantitative data on this relationship were recently summarized and critically discussed in review papers.<sup>7,36,37</sup> For example,

the dependence of the strengthening/embrittling energy (for definition, see Eq. (6) in Part III) on the difference of the sublimation enthalpies of host iron and solute elements is shown in Fig. 1.<sup>7</sup> The anisotropic effect of fracture propagation in S-doped nickel confirmed that the crack tends to propagate along general grain boundaries while low-angle, special and twin grain boundaries are more resistant against the fracture damage.<sup>22</sup> From the viewpoint of the atomic size, it seems that the characteristic strengthening/embrittling energy is closely related to the ratio of atomic radii of the host and segregated atoms: the segregated atoms with larger radii than the host atom usually act as embrittlors and those with smaller radii act as cohesion enhancers.<sup>24</sup> Another approach shows that the decisive role in the segregation-induced changes of the cohesion consists in the tendency of individual solutes to bond breaking.<sup>25,34,37</sup> However, the strengthening/embrittling energy is defined as a difference of the segregation energies at the grain boundaries and at the free surface (for their definition, see Eq. (5) in Sec. III), and the surface segregation also plays an important role in changes of the cohesion.<sup>26</sup>

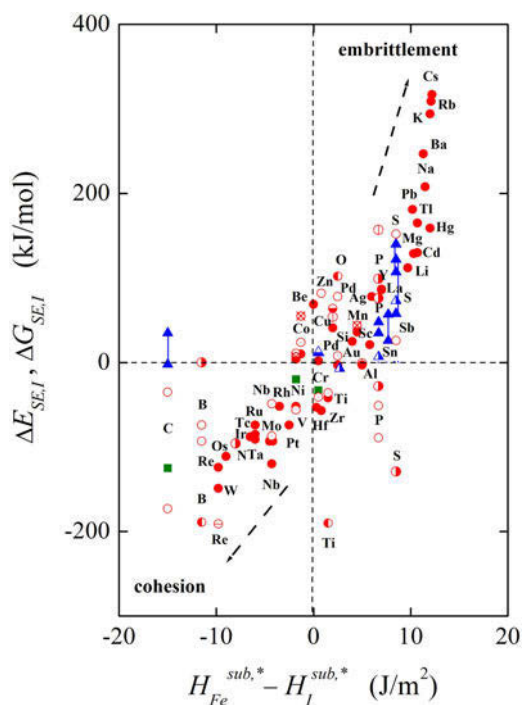


FIG. 1. Dependence of the strengthening/embrittling energy,  $\Delta E_{SE,I}$ , and/or the Gibbs energy,  $\Delta G_{SE,I}$ , on the difference of sublimation energies of  $\alpha$ -iron and respective solute. Blue triangles represent experimental data of  $\Delta G_{SE,I}$  at differently oriented grain boundaries. Symbols connected by vertical lines show limiting values of individual data. The red circles and green squares are the values calculated by DFT methods and by other theoretical approaches, respectively; the symbols of the same type correspond to the same source. Reprinted with permission from Ref. 7. Copyright 2017 Elsevier.

Despite the description of the solute segregation at interfaces seems to be well elaborated,<sup>8</sup> new models of grain boundary segregation emphasizing the role of entropy have been further developed which shed more light to individual dependences or refine the existing models. A new method was proposed to estimate energetic quantities of the grain boundary segregation on the basis of diffusion measurements in binary systems with limited solid solubility. Besides determining the grain boundary diffusivity, this method allows us to evaluate the characteristic parameters of the grain boundary segregation.<sup>38</sup> Kaptay<sup>39</sup> extended the Butler equation to model equilibrium energy and composition of grain boundaries in polycrystals. Based on the Cahn–Hilliard equation, a phenomenological model was proposed which describes different types of distribution of dissolved components as, e.g., depletion and/or enrichment of the grain boundary, and competitive precipitation in the bulk and at the grain boundary.<sup>40</sup> Additionally, a qualitative model has also been proposed to explain the contradiction between theoretical calculations of preferentially substitutional segregation of phosphorus at the grain boundaries of iron at 0 K and experimental indications of its interstitial segregation: This model is based on consideration of temperature dependence of the Gibbs energy of segregation for both positions in the grain boundary core and suggests the existence of a transition of the segregation site in the grain boundary core.<sup>41</sup> The importance of entropy in quantitative thermodynamic considerations has also been emphasized in the prediction of the grain boundary segregation<sup>42</sup> (and also in classification of grain boundaries on the basis of their chemical composition<sup>43</sup>). Practical importance of the entropy in the grain boundary segregation was documented on above-mentioned stabilization of the nanocrystalline structure in multicomponent nickel-based alloys containing particles of high-entropy alloys.<sup>15</sup>

Both the grain size stabilization and the relationship between the grain boundary segregation and changes of the intergranular cohesion can be successfully applied in the concept of the GBE. In this respect, a new specific branch—grain boundary segregation engineering—has been proposed.<sup>44–46</sup> According to this concept, solute segregation is utilized to manipulate specific grain boundary structures, compositions, and properties to enable optimum material behavior.<sup>45</sup> This effect is documented for example by Mn containing maraging steel in which ductile and tough martensite is produced.<sup>44,46</sup>

Further progress has also been made in the concept of grain boundary complexions during last five years. Present knowledge on grain boundary complexions was thoroughly summarized with respect to their categorization and transitions.<sup>47,48</sup> In this respect, bilayer grain boundary complexions and their faceting were observed and described in Cu–Bi alloys.<sup>49</sup> These bilayers were

found to be the main cause for significantly enhanced liquid metal embrittlement and corrosion.<sup>21</sup> Stable grain boundary complexions are also formed in polycrystalline alumina when the boundaries are enriched by yttrium, lanthanum, and/or magnesium. The values of the segregation energy at selected grain boundaries by the force field-based energy minimization method suggest that there is a critical solute concentration (3–4 atoms/nm<sup>2</sup>) for achieving the monolayer grain boundary complexion with the lowest mobility. Twin grain boundaries were found to be more favorable than general high angle grain boundaries to form monolayer complexions necessary for limiting grain growth.<sup>50</sup>

Recent effort in the field of nonequilibrium grain boundary segregation has been focused on the establishment of a unified mechanism of nonequilibrium segregation and segregation-induced embrittlement. This mechanism based on thermally induced and/or stress-induced nonequilibrium grain boundary segregation describes three types of intergranular embrittlement—reverse temper embrittlement of steels, intergranular corrosion embrittlement of stainless steels, and intermediate temperature embrittlement of metals and alloys.<sup>51</sup> These problems represent a consequence of an interim substantial increase of the grain boundary concentration of a harmful solute before it approaches an equilibrium value. For example, this mechanism is responsible for the embrittlement of Bi-doped nickel<sup>52</sup> and for loss of hot ductility of various stainless steels.<sup>53</sup> To overcome the problems of embrittling the steels, it was suggested to avoid slow cooling of the material from the aging temperature or keeping it at intermediate temperatures.<sup>54</sup>

However, the grain boundary segregation is not limited to metals and alloys which represent the earliest studied materials in many respects. Besides them, other materials have recently been studied in relationship to grain boundary segregation. In this connection, main attention has been paid to oxides like ZrO<sub>2</sub>,<sup>55–60</sup> TiO<sub>2</sub>,<sup>61–63</sup> CeO<sub>2</sub>,<sup>55,64</sup> UO<sub>2</sub>,<sup>65</sup> and ZnO<sup>66</sup>; as well as to silicon,<sup>67</sup> ferrites,<sup>68–70</sup> perovskites,<sup>71</sup> spinels,<sup>72</sup> and multiferroics.<sup>73</sup> A phenomenological model was proposed to explain the origin of grain boundary complexions and the first-order complexion transitions which may occur in CuO-doped TiO<sub>2</sub> bicrystals.<sup>61</sup> In these materials, the effect of segregation on their electric and magnetic properties have been frequently studied.<sup>64,66–69,71,73,74</sup> Hydrothermal stability, mechanical stability, and translucency were studied in materials for dental applications such as 3Y-TZP ceramics.<sup>57</sup> Considerable attention has been paid to the site of the segregant in the grain boundary core, i.e., which atom is substituted there.<sup>60,61,65,71</sup> It was also found that energetically stable configurations of the segregants vary in dependence on their ionic radii.<sup>56,58</sup> Although ZnO with high portion of grain boundaries can exhibit ferromagnetism itself, doping with “magnetic

atoms” such as manganese, cobalt, iron, or nickel, and their segregation facilitates its appearance.<sup>66</sup>

For the study of the grain boundary segregation and mainly its fine features, a feasible experimental tool is required. Therefore, further development of methodology and top instrumental equipment—high-resolution electron microscopy (HRTEM) and 3D atom probe tomography (3D APT)—has been reported recently. At present, the best atomic resolution at the interfaces is reached by spherical aberration-corrected scanning transmission electron microscopy (Cs-corrected STEM), which was applied for the first time in the study of chlorine and oxygen segregation at the grain boundaries in copper interconnects.<sup>75</sup> Aberration-corrected high-angle annular dark-field imaging in transmission electron microscopy was used to distinguish fine details of distribution of Hf atoms in the grain boundary core of Al<sub>2</sub>O<sub>3</sub>; it was proved that apparent multiple layer segregation is, in fact, single-layer segregation on the faceted grain boundary.<sup>76</sup> Solute segregation to inversion domain boundaries in ZnO was used as an example of the best procedure of transformation of obtained nanobeam-mode spectra to quantify the areal density of atoms contained within a very thin layer of a matrix material with a precision better than 1 atom/nm<sup>2</sup> in all these cases.<sup>77</sup> In contrast to HRTEM which provides us with site resolution of segregants at the grain boundary, 3D APT displays the distribution of the segregants in a relatively large volume (i.e., volume of the order of 10<sup>3</sup> cubic nanometers) inside the material albeit not identifying the site in the grain boundary core.<sup>78</sup> Therefore, it is a very important tool in studies of the grain boundary segregation mainly in nanocrystalline materials as done, for example, in the cases of characterization of the A15 phase in a bronze-route Nb<sub>3</sub>Sn superconducting wire with a Cu–Sn(Ti) bronze matrix,<sup>79</sup> of analysis of solute redistribution in pearlitic steel,<sup>80</sup> and of distribution of boron and alloying elements at prior austenite grain boundaries in a quenched martensitic steel.<sup>81</sup> A simplified nondestructive 3D electron backscatter diffraction (EBSD) methodology was proposed which enables us to measure all five degrees of freedom of grain boundaries combined with segregation analysis using 3D APT. The approach is based on two 2D EBSD measurements on orthogonal surfaces at a sharp edge of the specimen followed by the analysis of the grain boundary composition using 3D APT.<sup>82,83</sup> Nevertheless, a more precise procedure for the preparation of the desired specimen to study grain boundaries in refractory metals with a dual focused ion beam/scanning electron microscope is still required.<sup>81</sup>

Last but not least, theoretical calculations of the segregation energy have been intensively performed during the period of 2013–2017, too. The systems representing both the technologically applied materials and materials with application potential in the near future have been studied. As expected, the main host element

for these studies is  $\alpha$ -iron,<sup>84–91</sup> followed by nickel<sup>92–97</sup> and aluminum.<sup>98–102</sup> Frequently, the systems based on tungsten<sup>24,25,103–107</sup> and molybdenum<sup>103,104,108,109</sup> have also been studied. BaZrO<sub>3</sub> represents the nonmetallic system of increasing interest in connection with impurity and solute segregation.<sup>110–115</sup> In vast majority of these cases, the DFT procedures have been applied. Some of the above studies were performed according to the pattern coined by Všíanská and Šob.<sup>116</sup> The qualitative progress in the development of the procedures for calculations of the segregation energy was done when the quantum mechanics (QM)-based methods were combined with molecular mechanical ones to enlarge the computational repeat cell by several orders of magnitude.<sup>102</sup> This approach enabled us to calculate the energetic characteristics of general grain boundaries having low symmetry which cannot be obtained with help of classical DFT methods. It was proven quantitatively that sulfur segregates interstitially at  $\Sigma 5$  (210) grain boundary of  $\alpha$ -iron. However, presence of chromium prevents its segregation.<sup>86</sup> While both sulfur and chromium segregate at different sites in the grain boundary core, this is a flagrant example of repulsive interaction during solute segregation in a multicomponent system. Despite it is known that substitutional alloying elements significantly affect the processes running in steels such as recrystallization and austenite-ferrite phase transformation, mechanisms of their interaction with the interfaces remain unexplored. DFT calculations of segregation of niobium, molybdenum, and titanium at grain boundaries in iron suggest the co-segregation of these solutes at intermediate distances.<sup>87</sup> A new approach was proposed to design Ni-based polycrystalline superalloys: This approach is based on the idea that the creep-rupture characteristics of a superalloy are mostly determined by the strength of interatomic bonding at grain boundaries and in the bulk of the  $\gamma$  matrix. From this point of view, Zr, Hf, Nb, Ta, and B are proposed as the most promising low-alloying additions.<sup>93</sup> The calculated strengthening/embrittling energies of numerous solutes at nearly  $\Sigma 3$  (111) [110] tilt symmetric grain boundary in tungsten suggest that solutes with larger atom radius than tungsten, i.e., Sr, Th, In, Cd, Ag, Sc, Au, Ti, and Zn, embrittle tungsten while those with smaller atom radius—Cu, Cr, and Mn—can be considered as cohesion enhancers.<sup>24</sup> Besides them, boron, carbon, and beryllium were identified as potential alloying additions for an increased intergranular cohesion in tungsten and molybdenum. Similar to previously studied solute segregation at grain boundaries of nickel host,<sup>116</sup> calculations of the grain boundary and surface segregation energies in cobalt suggested that interstitially segregated Si should be the cohesion enhancer of the  $\Sigma 5$  (210) grain boundary while interstitially segregated S, Ge, As, and Se, and substitutionally segregated Ga, In, Sn, Sb, and Te are grain boundary embrittlors; interstitially segregated P and

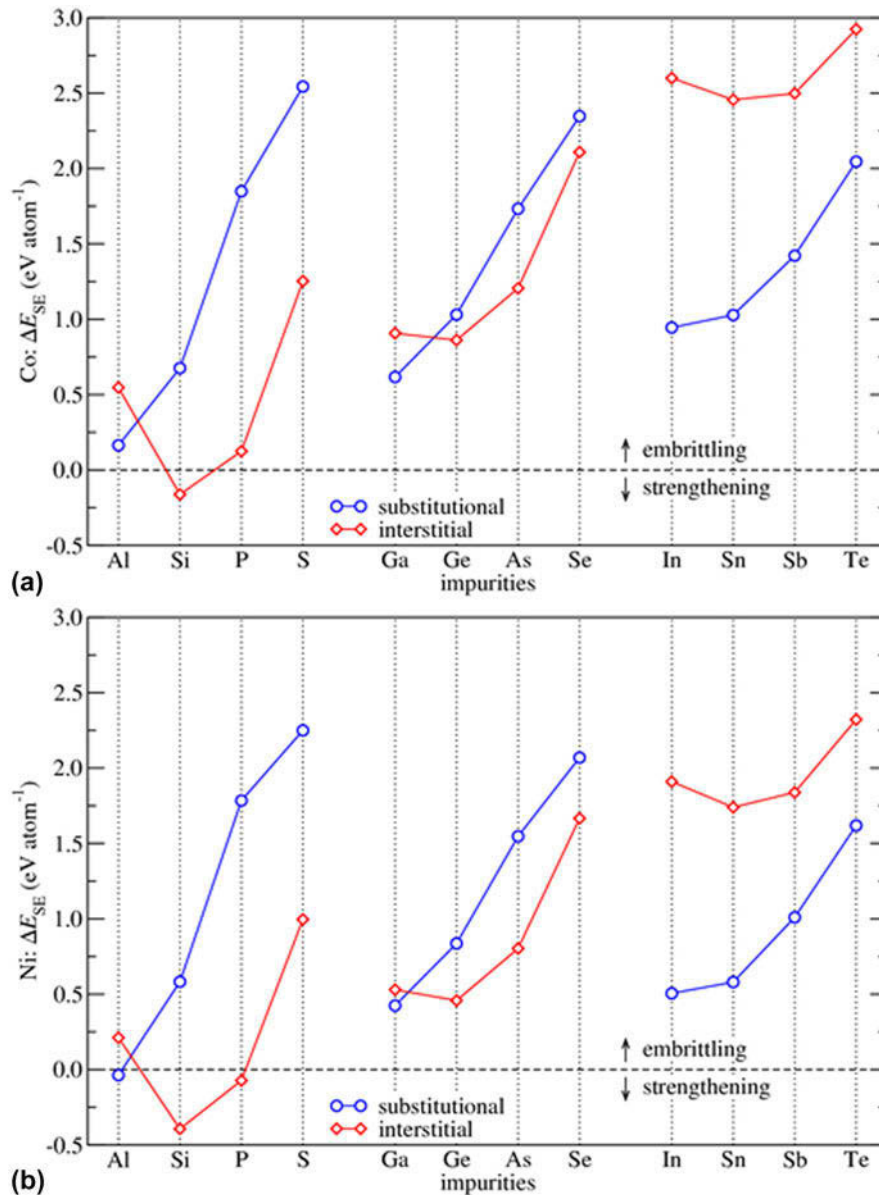


FIG. 2. Strengthening/embrittling energy,  $\Delta E_{SE}$ , at the  $\Sigma 5$  (210) GB in fcc Co (a) and Ni (b). Reprinted with permission from Ref. 97. Copyright 2017 IOP Publishing.

substitutionally segregated Al have a very small effect on the grain boundary cohesion (Fig. 2).<sup>97</sup> Unfortunately, a very important characteristic of the grain boundary segregation—segregation entropy—has not been calculated despite its importance was unambiguously proved.<sup>8,41,42</sup> It is also interesting that some solutes were found to change their site in the grain boundary core from substitutional to interstitial upon segregation.<sup>104</sup>

### III. OPEN QUESTIONS IN GRAIN BOUNDARY SEGREGATION

Substantial progress in understanding the grain boundary segregation, in development of the

experimental techniques enabling its study and mainly in calculation of the segregation energies has been done during the last five years. However, with this achievement, new questions have been opened which need to be addressed. Examples of such questions are as follows: Why there is an extreme disagreement in the values of the segregation energies for some solutes while there is quite a good agreement for others in the same host metal? What is the segregation site of individual solutes in the grain boundary core (mainly for metalloids in transition metals)? What is the role of the entropy in grain boundary segregation? Here, we will touch these questions and formulate some conclusions and consequences.

### A. Comparison of theoretical energies of grain boundary segregation with experimental values of segregation enthalpy

The majority of the experimental data are correlated according to the Langmuir–McLean segregation isotherm. This type of description deals with characteristic thermodynamic quantity of the grain boundary segregation, the molar Gibbs energy of segregation,  $\Delta G_I$ . In general, this isotherm can be written as<sup>8</sup>

$$\frac{X_I^{\text{GB}}}{X^0 - X_I^{\text{GB}}} = \frac{X_I}{1 - X_I} \exp\left(-\frac{\Delta G_I}{RT}\right), \quad (1)$$

where  $X_I^{\text{GB}}$  and  $X_I$  are the grain boundary and bulk concentrations of the solute I in a binary M–I solid solution,  $X^0$  is the saturation level of the grain boundary segregation,  $R$  is the universal gas constant, and  $T$  is the temperature.  $\Delta G_I$  is composed of two terms, the standard (ideal) molar Gibbs energy of segregation,  $\Delta G_I^0$ , and the excess molar Gibbs energy of segregation,  $\Delta G_I^E$ ,

$$\Delta G_I = \Delta G_I^0 + \Delta G_I^E. \quad (2)$$

Let us note that the standard state is chosen as the unperturbed bulk pure substance (i.e., element and—in the case of the host—also chemical compound, intermetallic compound, etc.) at the temperature  $T$  at which the segregation is studied, and under normal pressure in the structure of the host material, M. The other term on the right-hand side of Eq. (2),  $\Delta G_I^E = RT \ln \frac{\gamma_I^{\text{GB}} \gamma_M}{\gamma_I \gamma_M^{\text{GB}}}$ , is a combination of the corresponding activity coefficients,  $\gamma_i^\xi$ , reflecting the difference between ideal and real behavior,  $a_i^\xi = \gamma_i^\xi X_i^\xi$ , where  $a_i^\xi$  are the activities (i.e., generalized concentrations) of  $i$  in the state  $\xi$ .<sup>8</sup> As their values are hardly measurable,  $\Delta G_I^E$  is usually evaluated according to a suitable model. The Fowler approach is frequently used to approximate the effect of activity coefficients in binary systems, using a coefficient of binary interaction of I–I in M,  $\alpha_{I(M)}$ ,

$$\Delta G_I^E = -2\alpha_{I(M)}(X_I^{\text{GB}} - X_I). \quad (3)$$

The molar Gibbs energy of segregation,  $\Delta G_I$ , controls the grain boundary composition in binary M–I solid solution at temperature,  $T$ , and volume solute concentration,  $X_I$ . Unfortunately, it depends on  $X_I$ , and in a non-trivial way on  $T$  because of temperature dependence of  $X_I^{\text{GB}}$  and thus, it can hardly be extrapolated.

As the Gibbs energy,  $G$ , is composed of two terms, enthalpy,  $H$ , and entropy,  $S$ ,<sup>8,117</sup>

$$G = H - TS, \quad (4)$$

and—as was shown recently<sup>8,117</sup>— $\Delta H_I^0$  and  $\Delta S_I^0$  are independent of temperature, therefore, according to

Eq. (4),  $\Delta G_I^0$  is a linear function of temperature. According to the choice of the standard state,  $\Delta G_I^0$  is independent of  $X_I$  and therefore it can be well extrapolated. However, it describes  $X_I^{\text{GB}}$  only if  $\Delta G_I^E = 0$ , i.e., in an ideal or infinitesimally diluted system.<sup>8,117</sup>

The characteristic quantity used in theoretical approaches to the grain boundary segregation is the Helmholtz energy of segregation,  $\Delta F_I$ . This energy represents the difference between the energy of the system with the solute atom located at the grain boundary and the system with the same atom located in the bulk. However, the calculations of the interfacial segregation are frequently performed at 0 K (MS, DFT) and thus, only the internal energy of segregation,  $\Delta E_I^\Phi$ , is determined,

$$\Delta E_I^\Phi = E_I^\Phi - E_I^b, \quad (5)$$

where  $E_I^\Phi$  is the energy of the computational repeat cell with the atom I located at the interface ( $\Phi = \text{GB}$  for the grain boundary or FS for the free surface), and  $E_I^b$  is the energy of the same cell with the atom I located in the bulk. It is apparent from the definition that  $\Delta E_I$  reflects the real state of the grain boundary segregation. However, the recent analysis<sup>7</sup> showed that with a reasonable precision,  $\Delta H_I^0$  and  $\Delta E_I$  can be well compared as their difference,  $\Delta H_I^0 - \Delta E_I = PdV_I^E$ , is negligible at normal pressure.<sup>42</sup>

A recently published comparison of the values of the theoretically calculated segregation energy,  $\Delta E_I$ , and experimental values of the standard segregation enthalpy,  $\Delta H_I^0$ , showed that there exists an extreme disagreement between them for some solutes in iron and nickel, whereas some solutes exhibit very good agreement.<sup>7,118</sup> The plot of these values characterizing the grain boundary segregation against the solid solubility of the particular solute I,  $X_I^*$ , in  $\alpha$ -iron (represented by the Gibbs energy of solution,  $\Delta G_I^{\text{sol}} = RT \ln X_I^*$ ) showed two distinct areas—one of a very good agreement for well soluble solutes ( $X_I^* > 0.01$ ) while the other one exhibiting substantial disagreement for less soluble solutes ( $X_I^* < 0.01$ ), see Fig. 3.

The level of the limiting concentration,  $X_I^* \approx 0.01$ , coincides obviously with the “concentration” of a single atom in the computational repeat cell: In DFT calculations, the number of atoms in the computational supercell is usually close to 100 so that  $X_I \approx 0.01$ . If the solid solubility of the solute is lower than this concentration limit, the configuration of the system with the solute atom placed in the bulk is nonequilibrium one and, consequently, the segregation energy,  $\Delta E_I$ , involving  $E_I^b$  is also nonequilibrium one, i.e., it has no physical meaning. Of course, it is hard to compare a block with a single atom in a cell containing 100 atoms with the system containing say billions of atoms where the concentration has a real



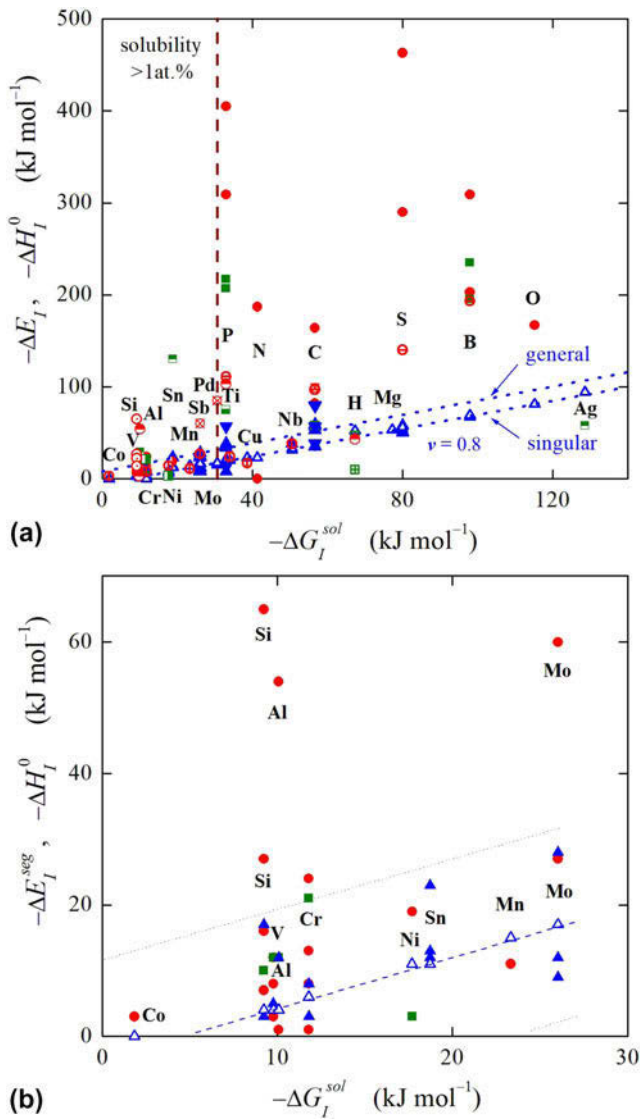


FIG. 3. Plot of the segregation energy and/or enthalpy of grain boundary segregation,  $\Delta E_I$  and  $\Delta H_I^0$ , versus the Gibbs energy of solution,  $\Delta G_I^{\text{sol}} = RT \ln X_I^*$  (i.e., solid solubility,  $X_I^*$ ), in  $\alpha$ -Fe. (a) Complete dependence; (b) detail for solutes with high solid solubility ( $X_I^* > 0.01$ ). Solid triangles: experimental data (AES, FIM, 3D APT); empty triangles and/or dashed lines: (experimental) prediction [in (a), it is prediction for solute segregation at general (upper line) and special (bottom line) grain boundaries]; dotted lines in (b): extent of the error of the values determined experimentally; solid circles: DFT values; solid squares: other theoretical values (MS, TB). Reprinted with permission from Ref. 7. Copyright 2017 Elsevier.

meaning. On the other hand, the computational supercell may represent the system quite well, and it is supposed that it is periodically repeated in the space so that we can imagine that a system can be formed by a solute creating, e.g., a “nanowire” through the lattice. If we consider only a single atom in the cell, we cannot in principle account for any interaction between two solute atoms, i.e., an important contribution to the energy of the bulk and

consequently segregation energy is completely omitted. The objections that the computation converges to a single value do not explain this problem as it can converge to a local minimum which can be far from the correct energy of the bulk system,  $E_I^b$ . However, despite the fact that some characteristics of interfacial segregation calculated for low-solubility segregants are unreliable due to physically meaningless values of  $E_I^b$  in Eq. (5), we can reliably determine the strengthening/embrittling energy,  $\Delta E_{\text{SE,I}}$ , which refers on the effect of the segregant to the changes of the intergranular cohesion, as this incorrectly determined term is removed,

$$\begin{aligned} \Delta E_{\text{SE,I}} &= \Delta E_I^{\text{GB}} - \Delta E_I^{\text{FS}} = (E_I^{\text{GB}} - E_I^b) - (E_I^{\text{FS}} - E_I^b) \\ &= E_I^{\text{GB}} - E_I^{\text{FS}} \end{aligned} \quad (6)$$

Nevertheless, the discussion about the reliability of the segregation energy is still open and needs proofs, tests, and final answering.

## B. Solute site in the grain boundary core: interstitial or substitutional?

One of the examples of a solute exhibiting large scatter of the data shown in Fig. 3(a) is phosphorus. However, the solid solubility of phosphorus in the volume of  $\alpha$ -iron is rather close to the limit value of  $X_I^* \approx 0.01$ . One of the sources of surprisingly large scatter among the theoretical values of  $\Delta E_I$  for a single grain boundary is the considered site of the segregated atom in the grain boundary core. Phosphorus is a substitutional solute in bulk  $\alpha$ -iron and frequently, it is a priori accepted as the substitutional segregant.<sup>119–121</sup> Despite that, it is also sometimes a priori considered as the interstitial segregant.<sup>5,122,123</sup> In some theoretical papers, the calculated values of  $\Delta E_P$  for both interstitial and substitutional sites are compared to show the site preference (lower segregation or binding energy indicates the preference of the site). Yamaguchi’s calculations provide a quantitative evidence for the preference of substitutional segregation in the second boundary layer (as read from the figures,  $\Delta E_P \cong -80$  kJ/mol for interstitial and  $\Delta E_P \cong -110$  kJ/mol for substitutional segregation at  $\Sigma 3\{111\}$  grain boundary of  $\alpha$ -iron)<sup>124</sup> although—compared to the reported accuracy of  $\pm 10$  kJ/mol of the determination of  $\Delta E_P$ , see Ref. 125—this difference is rather small. Rajagopalan et al.<sup>126</sup> report stable substitutional segregation position either in the 2nd or in the 3rd layer at numerous grain boundaries. Nearly the same values of  $\Delta E_P$  for substitutional segregation in the 2nd layer and for interstitial segregation at the  $\Sigma 3\{111\}$  grain boundary of  $\alpha$ -iron is reported by Ko et al.<sup>127</sup> although they claim that substitutional segregation is preferred. On the other hand, interstitial segregation is preferred elsewhere. Braithwaite and Rez<sup>128</sup> refer

the interstitial position to be more stable at the  $\Sigma 5\{210\}$  grain boundary than the substitution position in the 2nd layer; however, for calculations of the exchange and correlation energy, they applied the local density approximation which does not describe the energetics of iron correctly. Wachowicz and Kiejna<sup>129</sup> report distinctly different values of  $\Delta E_p$  for substitutional and interstitial segregation at  $\Sigma 3\{111\}$  grain boundary (about  $-15$  kJ/mol and about  $-310$  kJ/mol, respectively) as well as for  $\Sigma 5\{210\}$  grain boundary (about  $-80$  kJ/mol and about  $-405$  kJ/mol, respectively). However, the values given for the interstitial segregation are too low (i.e., too large in absolute value) to describe the segregation correctly.<sup>7</sup> Our own preliminary calculations<sup>130</sup> show that the interstitial position is stable at the  $\Sigma 5\{210\}$  grain boundary while the substitutional position is unstable. We also compared energetics of phosphorus segregation in the substitutional position in the 2nd layer and in the interstitial position directly at the  $\Sigma 3\{111\}$  grain boundary. In comparison with Yamaguchi,<sup>124</sup> we used a more precise setting for our calculations. Contrary to Yamaguchi,<sup>124</sup> we obtained nearly the same energetic values for both positions with a slight preference for the interstitial position at the grain boundary.

On the other hand, indirect experimental evidence based on the enthalpy–entropy compensation effect suggests interstitial segregation of phosphorus.<sup>41,117</sup> In its integral form, the enthalpy–entropy compensation effect for grain boundary segregation (which is also reported in more detail in Sec. III.C) is represented by a linear dependence between the standard enthalpy,  $\Delta H_I^0$ , and standard entropy,  $\Delta S_I^0$ , of grain boundary segregation,<sup>8,117</sup>

$$\Delta S_I^0 = \frac{\Delta H_I^0}{T_{CE}} + \Delta S' \quad , \quad (7)$$

where  $\Delta S'$  is the integration constant. In the case of the grain boundary segregation in  $\alpha$ -iron, expression (7) is well fulfilled by various solutes (Fig. 4). It is apparent from Fig. 4 that this dependence splits into two branches, the upper one for interstitial segregants and the lower one for substitutional solutes. Accordingly, phosphorus, tin, antimony, and probably also other metalloids may be supposed to segregate interstitially at the grain boundaries of  $\alpha$ -iron. Let us note that not only the experimental results but also theoretical values of Ko et al.<sup>131</sup> on temperature dependence of the grain boundary concentrations at three different grain boundaries calculated by the MC approach using a modified embedded-atom method which provide us with the values of the segregation enthalpy and entropy, fit with the interstitial branch in Fig. 4.

It is apparent from the above survey that the position of the segregated phosphorus at the grain boundaries of

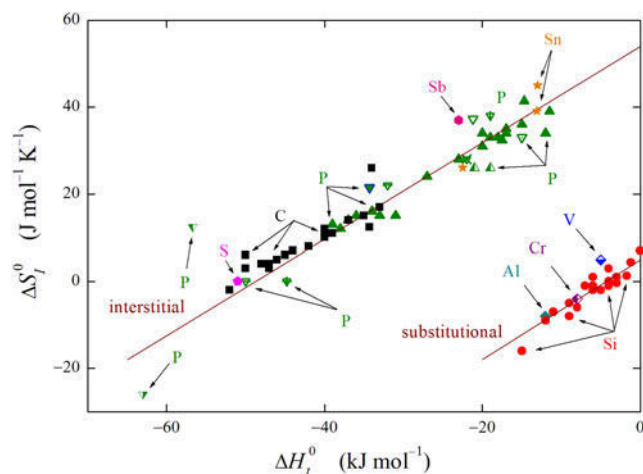


FIG. 4. Integral form of the enthalpy–entropy compensation effect for grain boundary segregation in  $\alpha$ -iron. Full symbols: segregation of C (squares), P (triangles), and Si (circles) at individual grain boundaries. Other symbols are literature data for solute segregation in polycrystalline  $\alpha$ -Fe.<sup>41,117</sup> Theoretical values according to Ko et al.<sup>131</sup> are the half-solid triangles at the right-hand side of the figure just under the interstitial branch (denoted by nearly horizontal arrow for P). Reprinted with permission from Ref. 41. Copyright 2016 IOP Publishing.

$\alpha$ -iron is not clearly determined at all. Some theoretical results show qualitative agreement with experimental deductions; however, quantitatively, there is a large discrepancy. The other theoretical values contradict with the experiment, although according to Yamaguchi,<sup>124</sup> the difference between the substitutional and interstitial position should be small.

### C. Role of entropy in grain boundary segregation

It is apparent from Part B that the entropy is an important thermodynamic variable also in grain boundary segregation. Unfortunately, this parameter is not used regularly in the segregation considerations; better say, it is frequently (or nearly always) neglected. Probably, it is the consequence of the fact that the procedure of its theoretical calculation is complicated or has not been elaborated yet and that it represents an additional variable for evaluation of experimental data.

We did already see that the entropy plays an important role in explanation of the site preference in the grain boundary segregation. This example as well as other confirmations result from the existence of the enthalpy–entropy compensation effect.<sup>8,42,117</sup> In fact, Eq. (7) is only an integral form which seems to suggest that entropy and enthalpy are mutually dependent. However, it is not so—the enthalpy–entropy compensation effect says that the changes of enthalpy caused by a changed intensive parameter (here the grain boundary structure,  $\Psi$ ) are compensated by the changes of the entropy caused by the same change of that parameter,<sup>8,117</sup>



$$T_{CE} = \frac{\left(\frac{\partial \Delta H_1^0(\Psi)}{\partial \Psi}\right)_{T,P}}{\left(\frac{\partial \Delta S_1^0(\Psi_1)}{\partial \Psi}\right)_{T,P}} \quad (8)$$

In fact, the  $T_{CE}$  represents the reciprocal value of the slope of the enthalpy–entropy compensation effect shown in Fig. 4. The value of  $T_{CE}$  for ferritic iron is 900 K and is identical for both branches of this dependence, i.e., for substitutional as well as interstitial segregants.<sup>41,117</sup> Unfortunately, this is the only host for which the value of  $T_{CE}$  was determined till now as there is no sufficient information on the values of the segregation entropy for solutes in other hosts.

The direct consequence of Eq. (8) combined with Eq. (4) is that at compensation temperature,  $T_{CE}$ ,  $d\Delta G_1^0 = 0$ , i.e.,  $\Delta G_1^0 \neq f(\Psi)$ . This means that at  $T_{CE}$ , all grain boundaries in a polycrystal possess the same composition. This also means that the magnitude of the anisotropy of grain boundary composition observed at low temperatures is reduced if temperature approaches  $T_{CE}$  and disappears at  $T_{CE}$ . Above  $T_{CE}$ , the anisotropy of solute segregation is reversed, i.e., general boundaries which exhibited stronger segregation at lower temperatures that special ones, possess lower solute concentrations at high temperatures (Fig. 5).<sup>43</sup> On its basis, for example, anomalous structural dependence of silicon segregation at grain boundaries of a stainless steel (i.e., maximum silicon segregation at special  $\{013\}$ ,  $\{012\}$ , and  $\{023\}$  grain boundaries) was explained.<sup>8,43</sup>

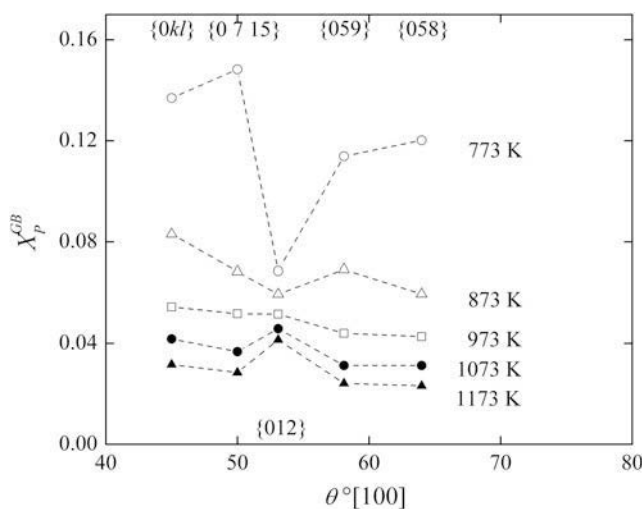


FIG. 5. Dependence of atomic fraction of phosphorus at  $[100]$  symmetric tilt grain boundaries,  $X_P^{GB}$ , in Fe–3.55 at.% Si–0.0089 at.% P–0.014 at.% C alloy on misorientation angle,  $\theta$ , at various temperatures.  $45^\circ [100]$ ,  $\{0kl\}$  is the incommensurate symmetrical tilt grain boundary for which  $k/l$  is irrational. Reprinted with permission from Ref. 43. Copyright 2010 Elsevier.

The enthalpy–entropy compensation effect is a very important phenomenon and is of general thermodynamic validity. It has been observed in many other areas of material science, chemistry, biology, etc. Examples of these processes are not only solute segregation at free surfaces and grain boundaries but also grain boundary diffusion and migration, dislocation glide, hydrogen bonding, crystal melting, formation of van der Waals complexes, solubility, micellization, adsorption, enantiomer separation, gas and liquid chromatography, water sorption, solvation, thermal transitions, solution extraction, polymer degradation, conformational equilibrium, ionic hydration, dielectric relaxation, antibiotic dissociation, enzyme binding, catalysis, thermal death of microorganisms, depolymerization of food saccharides, cucumber tissue softening, nonenzymatic browning of potato strips, and conductance of transistors.<sup>8,117</sup>

The above considerations have a very important consequence—they clearly emphasize the necessity to consider entropy in the grain boundary segregation albeit it has been frequently omitted. The segregation entropy was already shown to be important in the above mentioned reversion of the anisotropy of grain boundary segregation which has serious consequences, e.g., for the classification of individual high-angle grain boundaries<sup>8,43</sup> and prediction of grain boundary segregation.<sup>8,41,117,132</sup> In our opinion, it is necessary to find effective procedures for computing the segregation entropy and determine the missing values: only in this case, we will be able to deal reasonably with grain boundary segregation. Let us document it on the classical example of phosphorus segregation at grain boundaries in ferritic iron. The data were measured by Erhart and Grabke<sup>133</sup> for various bulk concentrations of phosphorus at temperatures ranging between 400 and 900 °C. The correlation of the temperature dependence of phosphorus grain boundary concentration for the bulk concentrations  $X_P = 0.0017$  provides us with the values of segregation enthalpy,  $\Delta H_P^0 = -36$  kJ/mol, and segregation entropy,  $\Delta S_P^0 = 22$  J/(mol K). (Erhart and Grabke give the values  $\Delta H_1^0 = -34.3$  kJ/mol and  $\Delta S_1^0 = 21.5$  J/(mol K) which were averaged for all bulk concentrations used.) This is documented in Fig. 6 by red circles and solid red line. If the segregation entropy is neglected and the correlation of the experimental data is done only by “effective” segregation enthalpy,  $\Delta H_P^{eff} = -55$  kJ/mol, representing the “best fit” of the experimental data (blue dashed line in Fig. 6), we see that this line does not fit the experimental data properly. This comparison shows that the segregation entropy cannot be neglected in the case of accurate considerations. From this point of view, the calculations of the grain boundary concentration based exclusively on the use of the segregation energy calculated for 0 K by DFT methods as it is sometimes presented,<sup>90,124,134</sup> are doubtful and thus unreliable.

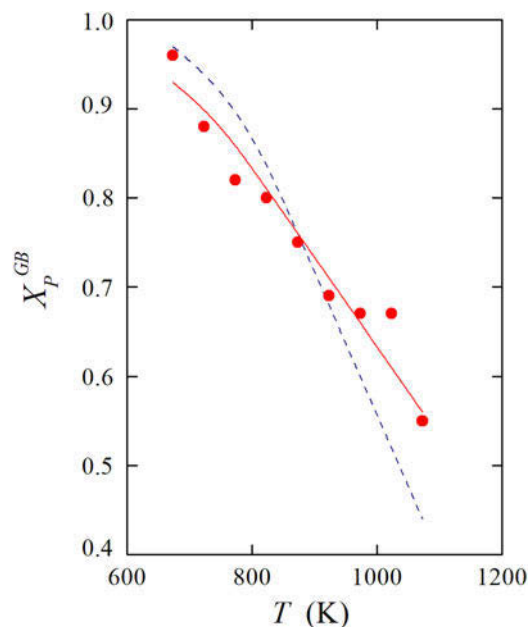


FIG. 6. Temperature dependence of phosphorus grain boundary segregation in iron as measured by Erhart and Grabke.<sup>133</sup>  $X_P = 0.0017$ . Red circles are the experimental grain boundary concentrations and solid red line represents the fit of the data with  $\Delta H_1^0 = -36$  kJ/mol and  $\Delta S_1^0 = 22$  J/(mol K); blue dashed line is the fit of the data using an effective enthalpy of segregation,  $\Delta H_1^{\text{eff}} = -55$  kJ/mol without considering the segregation entropy

Additionally, consideration of the entropy enables us to shift the understanding of the grain boundary segregation and all connected fields to a higher level as it is indispensable in explanation of many effects, which have not been solved yet.

#### IV. CONCLUSIONS

The progress achieved in the field of the grain boundary segregation during last five years (2013–2017) was presented and discussed in this paper. Fundamental progress has been achieved mainly in stabilization of nanocrystalline structures by grain boundary segregation, in the concept of grain boundary complexes and in GBE where a new branch of grain boundary segregation engineering was formulated. Great attention was also paid to the development of both experimental techniques to study grain boundary segregation and computational procedures of determination of the segregation energy. In the latter case, the combination of the MD and QM seems to be the most promising tool for overcoming many objections connected with calculations of the segregation energy. The study of the segregation is not limited to metallic hosts but has been gradually extending to other materials like ceramics, multiferroics, semiconductors, oxides, and silicon. However, every progress opens new questions

which need to be addressed. Here we did touch three problems: (i) comparison of the theoretical calculations of the segregation energy and experimental results of the segregation enthalpy; (ii) site preference of metalloids in the grain boundary core; and (iii) the role of entropy in the grain boundary segregation. In these areas, we show possible reasons of difficulties but we are aware that they require further effort to reach final explanation. We demonstrate here that a great attention should be paid to reliability of the obtained data. A special problem is the segregation entropy: it can be determined experimentally but theoretical information about it is very rare. However, it is a very important thermodynamic parameter which cannot be omitted in treatments of solute segregation as many questions cannot be answered without considering this quantity.

#### ACKNOWLEDGMENTS

This work was supported by the Czech Science Foundation [Projects Nos. GB P108/12/G043 (PL) and GA 16-24711S (MŠ, MV)], by the Academy of Sciences of the Czech Republic [Institutional Projects RVO:68378271 (PL) and RVO:68081723 (MŠ, MV)], and by the Ministry of Education, Youth and Sports of the Czech Republic under the project CEITEC 2020 (LQ1601) (MŠ, MV). Computational resources were provided by the Ministry of Education, Youth and Sports of the Czech Republic under the Projects CESNET (Project No. LM2015042), CERIT-Scientific Cloud (Project No. LM2015085), and IT4Innovations National Supercomputer Center (Project No. LM2015070) within the program Projects of Large Research, Development and Innovations Infrastructures.

#### REFERENCES

1. W. Hampe: Beiträge zu der Metallurgie des Kupfers. *Z. Berg-, Hütten- und Salinenwesen* **23**, 93 (1874).
2. M.T. Stewart, R. Thomas, K. Wauchope, W.C. Winegard, and B. Chalmers: New segregation phenomena in metals. *Phys. Rev.* **83**, 657 (1951).
3. E.D. Hondros, M.P. Seah, S. Hofmann, and P. Lejček: Surface and interfacial microchemistry. In *Physical Metallurgy*, 4th ed., R.W. Cahn and P. Haasen, eds. (North-Holland, Amsterdam, 1996); pp. 1201–1289.
4. D. Kalderon: Steam turbine failure at Hinkley point 'A'. *Proc. Inst. Mech. Eng.* **186**, 341 (1972).
5. M. Hashimoto, Y. Ishida, R. Yamamoto, and M. Doyama: Atomistic studies of grain boundary segregation in Fe–P and Fe–B alloys. I. Atomistic structure and stress distribution. *Acta Metall.* **32**, 1 (1984).
6. K. Masuda-Jindo: On the grain boundary segregation of sp-valence impurities in b.c.c. transition metal. *Phys. Status Solidi B* **134**, 545 (1986).
7. P. Lejček, M. Šob, and V. Paidar: Interfacial segregation and grain boundary embrittlement: An overview and critical assessment of experimental data and calculated results. *Prog. Mater. Sci.* **87**, 83 (2017).

8. P. Lejček: *Grain Boundary Segregation in Metals* (Springer, Berlin, 2010).
9. H.A. Murdoch and C.A. Schuh: Stability of binary nanocrystalline alloys against grain growth and phase separation. *Acta Mater.* **61**, 2121 (2013).
10. H.A. Murdoch and C.A. Schuh: Estimation of grain boundary segregation enthalpy and its role in stable nanocrystalline alloy design. *J. Mater. Res.* **28**, 2154 (2013).
11. T. Chookajorn and C.A. Schuh: Thermodynamics of stable nanocrystalline alloys: A Monte Carlo analysis. *Phys. Rev. B* **89**, 064102 (2014).
12. M. Saber, C.C. Koch, and R.O. Scattergood: Thermodynamic grain size stabilization models: An overview. *Mater. Res. Lett.* **3**, 65 (2015).
13. F. Abdeljawad and S.M. Foiles: Stabilization of nanocrystalline alloys via grain boundary segregation: A diffuse interface model. *Acta Mater.* **101**, 159 (2015).
14. T. Liang, Z. Chen, X. Yang, J. Zhang, and P. Zhang: The thermodynamic stability induced by solute co-segregation in nanocrystalline ternary alloys. *Int. J. Mater. Res.* **108**, 435 (2017).
15. N. Zhou, T. Hu, J. Huang, and J. Luo: Stabilization of nanocrystalline alloys at high-temperatures via utilizing high-entropy grain boundary complexions. *Scr. Mater.* **124**, 160 (2016).
16. J. Svoboda and F.D. Fischer: Abnormal grain growth: A non-equilibrium thermodynamic model for multigrain binary systems. *Modell. Simul. Mater. Sci. Eng.* **22**, 015013 (2014).
17. O. Waseda, H. Goldenstein, G.F.B. Lenz Silva, A. Neiva, P. Chantrenne, J. Morthomas, M. Perez, C.S. Becquart, and R.G.A. Veiga: Stability of nanocrystalline Ni-based alloys: Coupling Monte Carlo and molecular dynamics simulations. *Modell. Simul. Mater. Sci. Eng.* **25**, 075005 (2017).
18. T. Chookajorn and C.A. Schuh: Nanoscale segregation behavior and high-temperature stability of nanocrystalline W–20 at.% Ti. *Acta Mater.* **73**, 128 (2014).
19. F. Abdeljawad, P. Lu, N. Argibay, B.G. Clarke, B.L. Boyce, and S.M. Foiles: Grain boundary segregation in immiscible nanocrystalline alloys. *Acta Mater.* **126**, 528 (2017).
20. Z. Chen, F. Liu, X.Q. Yang, C.J. Shen, and Y.M. Zhao: A thermokinetic description of nano-scale grain growth under dynamic grain boundary segregation conditions. *J. Alloys Compd.* **608**, 338 (2014).
21. J. Luo: A short review of high-temperature wetting and complexion transitions with a critical assessment of their influence on liquid metal embrittlement and corrosion. *Corrosion* **72**, 897 (2016).
22. S. Kobayashi, T. Maruyama, S. Saito, S. Tsurekawa, and T. Watanabe: In situ observations of crack propagation and role of grain boundary microstructure in nickel embrittled by sulfur. *J. Mater. Sci.* **49**, 4007 (2014).
23. B. Djamel, R.L. Gall, and I.K. Lefkaier: Effect of small content and annealing temperature on the intergranular fracturing susceptibility of metallic nickel. *Surf. Rev. Lett.* **23**, 1650050 (2016).
24. Z.W. Li, X.S. Kong, L. Wei, C.S. Liu, and Q.F. Fang: Segregation of alloying atoms at a tilt symmetric grain boundary in tungsten and their strengthening and embrittling effects. *Chin. Phys. B* **23**, 106107 (2014).
25. D. Scheiber, V.I. Razumovskiy, P. Pusching, R. Pippan, and L. Romaner: Ab initio description of segregation and cohesion of grain boundaries in W–25 at.% Re alloys. *Acta Mater.* **88**, 180 (2015).
26. P. Lejček, P. Šandera, J. Horníková, P. Řehák, and J. Pokluda: Grain boundary segregation of elements of groups 14 and 15 and its consequences for intergranular cohesion of ferritic iron. *J. Mater. Sci.* **52**, 5822 (2017).
27. Y. Mehta, V.V. Dabhade, and G.P. Chaudhari: Effect of silicon and nitrogen on the microstructure and mechanical behavior of high-phosphorus steels. *Metallogr., Microstruct., Anal.* **5**, 384 (2016).
28. X. He, S. Wu, L. Jia, D. Wang, Y. Dou, and W. Yang: Grain boundary segregation of substitutional solutes/impurities and grain boundary decohesion in bcc Fe. *Energy Procedia* **127**, 377 (2017).
29. R.I. Babicheva, S.V. Dmitriev, L. Bai, Z. Ying, G. Kang, and K. Zhou: Effect of grain boundary segregation on the deformation mechanism and mechanical properties of nanocrystalline binary aluminum alloys. *Comput. Mater. Sci.* **117**, 445 (2016).
30. A.V. Zinovev, M.G. Bapanina, R.I. Babicheva, N.A. Enikeev, S.V. Dmitriev, and K. Zhou: Deformation of nanocrystalline binary aluminum alloys with segregation of Mg, Co and Ti at grain boundaries. *Phys. Met. Metallogr.* **118**, 65 (2017).
31. X. Sauvage, S. Lee, K. Matsuda, and Z. Horita: Origin of the influence of Cu and Ag micro-additions on the age hardening behavior of ultrafine-grained Al–Mg–Si alloys. *J. Alloys Compd.* **710**, 199 (2017).
32. I. Basu, K.G. Pradeep, C. Mießen, L.A. Barrales-Mora, and T. Salman: The role of atomic scale segregation in designing highly ductile magnesium alloy. *Acta Mater.* **116**, 77 (2016).
33. M.G. Jo, P.P. Madakashira, J.Y. Suh, and H.N. Han: Effect of nitrogen on microstructure and mechanical properties of vanadium. *Mater. Sci. Eng., A* **675**, 92 (2016).
34. S. Shi, L. Zhu, H. Zhang, and Z. Sun: Segregation effects of Y, Ti, Cr, and Si on the intergranular fracture of niobium. *J. Alloys Compd.* **711**, 637 (2017).
35. A.I. Kovalev, D.L. Wainstein, and A.Y. Rashkovskiy: Al grain boundary segregations in doped intermetallic NiAl and their effect on brittleness at room temperature. *Bull. Russ. Acad. Sci. Phys.* **80**, 1253 (2016).
36. M.A. Gibson and C. A. Schuh: Segregation-induced changes in grain boundary cohesion and embrittlement in binary alloys. *Acta Mater.* **95**, 145 (2015).
37. M.A. Gibson and C.A. Schuh: A survey of ab initio calculations shows that segregation induced grain boundary embrittlement is predicted by bond breaking arguments. *Scr. Mater.* **113**, 55 (2016).
38. V.A. Esin and Y. Souhar: Solvent grain boundary diffusion in binary solid solutions: A new approach to evaluate solute grain boundary segregation. *Philos. Mag.* **94**, 4066 (2014).
39. G. Kaptay: Modelling equilibrium grain boundary segregation, grain boundary energy and grain boundary segregation transition by the extended Butler equation. *J. Mater. Sci.* **51**, 1738 (2016).
40. P.E. L'vov and V.V. Svetukhin: Influence of grain boundaries on the distribution of components in binary alloys. *Phys. Solid State* **59**, 2453 (2017).
41. P. Lejček and S. Hofmann: Interstitial and substitutional solute segregation at individual grain boundaries of  $\alpha$ -iron: Data revisited. *J. Phys.: Condens. Matter* **28**, 064001 (2016).
42. P. Lejček, L. Zheng, S. Hofmann, and M. Šob: Applied thermodynamics: Grain boundary segregation. *Entropy* **16**, 1462 (2014).
43. P. Lejček, A. Jäger, and V. Gärtnerová: Reversed anisotropy of grain boundary properties and its effect on grain boundary engineering. *Acta Mater.* **58**, 1930 (2010).
44. D. Raabe, S. Sandlöbes, J. Millán, D. Ponge, H. Assadi, M. Herbig, and P.P. Choi: Segregation engineering enables nanoscale martensite to austenite phase transformation at grain boundaries: A pathway to ductile martensite. *Acta Mater.* **61**, 6152 (2013).
45. D. Raabe, M. Herbig, S. Sandlöbes, Y. Li, D. Tytko, M. Kuzmina, D. Ponge, and P.P. Choi: Grain boundary

- segregation engineering in metallic alloys: A pathway to the design of interfaces. *Curr. Opin. Solid State Mater. Sci.* **18**, 253 (2014).
46. M. Kuzmina, D. Ponge, and D. Raabe: Grain boundary segregation engineering and austenite reversion turn embrittlement into toughness: Example of a 9 wt% medium Mn steel. *Acta Mater.* **86**, 182 (2015).
  47. P.R. Cantwell, S.T. Ming, J. Dillon, J. Luo, G.S. Rohrer, and M.P. Harmer: Grain boundary complexions. *Acta Mater.* **62**, 1 (2014).
  48. S.J. Dillon, K. Tai, and S. Chen: The importance of grain boundary complexions in affecting physical properties of polycrystals. *Curr. Opin. Solid State Mater. Sci.* **20**, 324 (2016).
  49. A. Kundu, K.M. Asl, J. Luo, and M.P. Harmer: Identification a bilayer grain boundary complexion in Bi-doped Cu. *Scr. Mater.* **68**, 146 (2013).
  50. A. Tewari and P. Bowen: Grain boundary complexion and transparent polycrystalline alumina from an atomistic simulation perspective. *Curr. Opin. Solid State Mater. Sci.* **20**, 278 (2016).
  51. T. Xu, L. Zheng, K. Wang, and R.D.K. Misra: Unified mechanism of intergranular embrittlement based on non-equilibrium grain boundary segregation. *Int. Mater. Rev.* **58**, 263 (2013).
  52. L. Zheng, R. Chellali, R. Schlessinger, Y. Meng, D. Baither, and G. Schmitz: Identical mechanism of isochronal embrittlement in Ni(Bi) alloy: Thermo-induced non-equilibrium grain boundary segregation of Bi. *Appl. Surf. Sci.* **337**, 90 (2015).
  53. Z. Liu, H. Yu, K. Wang, and T. Xu: Non-equilibrium grain-boundary segregation mechanism of hot ductility loss for austenitic and ferritic stainless steels. *J. Mater. Res.* **30**, 2117 (2015).
  54. S.H. Song, Y. Zhao, and H. Si: Non-equilibrium phosphorus grain-boundary segregation and its effect on embrittlement in a niobium-stabilized interstitial-free steel. *Mater. Lett.* **140**, 20 (2015).
  55. H.B. Lee, F.B. Prinz, and W. Cai: Atomistic simulations of grain boundary segregation in nanocrystalline yttria-stabilized zirconia and gadolinia-doped ceria solid oxide electrolytes. *Acta Mater.* **61**, 3872 (2013).
  56. T. Yokoi, M. Yoshiya, and H. Yasuda: Nonrandom point defect configurations and driving force transitions for grain boundary segregation in trivalent cation doped ZrO<sub>2</sub>. *Langmuir* **30**, 14179 (2014).
  57. F. Zhang, K. Vanmeensel, M. Batuk, J. Hadermann, M. Inokoshi, B. Van Meerbeek, I. Naeret, and J. Vleugels: Highly-translucent, strong and aging resistant 3Y-TZP ceramics for dental restoration by grain boundary segregation. *Acta Biomater.* **16**, 215 (2015).
  58. T. Yokoi, M. Yoshiya, and H. Yasuda: On modeling of grain boundary segregation in aliovalent cation-doped ZrO<sub>2</sub>: Critical factors in site-selective point defect occupancy. *Scr. Mater.* **102**, 91 (2015).
  59. F. Zhang, M. Batuk, J. Hadermann, G. Manfredi, A. Mariën, K. Vanmeensel, M. Inokoshi, B. Van Meerbeek, I. Naert, and J. Vleugels: Effect of cation-dopant radius on the hydrothermal stability of tetragonal zirconia: Grain boundary segregation and oxygen vacancy annihilation. *Acta Mater.* **106**, 48 (2016).
  60. B. Feng, T. Yokoi, A. Kumamoto, M. Ikuhara, and N. Shibata: Atomically ordered solute segregation behavior in an oxide grain boundary. *Nat. Commun.* **7**, 11079 (2016).
  61. S. Ma, P.R. Cantwell, T.J. Pennycook, N. Zhou, M.P. Oxley, D.N. Leonard, S.J. Pennycook, J. Luo, and M.P. Harmer: Grain boundary complexion transitions in WO<sub>3</sub>- and CuO-doped TiO<sub>2</sub> bicrystals. *Acta Mater.* **61**, 1691 (2013).
  62. J.K. Yan, K.Y. Kang, and G.Y. Gan: Grain boundary segregation and the formation mechanism of secondary-phase in (Ce,Nb)-codoped TiO<sub>2</sub> ceramics. *Mater. Des.* **99**, 155 (2016).
  63. J.K. Yan, K.Y. Kang, J.H. Du, G.Y. Gan, and J.H. Yi: Grain boundary segregation and secondary-phase transition of (La,Nb) codoped TiO<sub>2</sub> ceramic. *Ceram. Int.* **42**, 11584 (2016).
  64. B. Meng, Z.L. Lin, Y.J. Zhou, Q.Q. Yang, M. Kong, and B.F. Meng: Effects of Fe-dopings through solid solution and grain-boundary segregation on the electrical properties of CeO<sub>2</sub>-based solid electrolytes. *Ionics* **21**, 2575 (2015).
  65. D.A. Andersson, M.R. Tonks, L. Casillas, S. Vyas, P. Nerikar, B.P. Ubruaga, and C.R. Stanek: Multiscale simulation of xenon diffusion and grain boundary segregation in UO<sub>2</sub>. *J. Nucl. Mater.* **462**, 15 (2015).
  66. B.B. Straumal, S.G. Protasova, A.A. Mazilkin, E. Goering, G. Schütz, P.B. Straumal, and B. Baretzky: Ferromagnetic behavior of ZnO: The role of grain boundaries. *Beilstein J. Nanotechnol.* **7**, 1936 (2016).
  67. A. Stoffers, O. Cojocaru-Mirédin, W. Seifert, S. Zaefferer, S. Riepe, and D. Raabe: Grain boundary segregation in multi-crystalline silicon: Correlative characterization by EBSD, EBIC, and atom probe tomography. *Prog. Photovoltaics Res. Appl.* **23**, 1742 (2015).
  68. R.A. Mondal, B.S. Murty, and V.R.K. Murthy: Maxwell-Wagner polarization in grain boundary segregated NiCuZn ferrite. *Curr. Appl. Phys.* **14**, 1727 (2014).
  69. R.A. Mondal, B.S. Murty, and V.R.K. Murthy: Temperature and frequency dependent electrical properties of NiCuZn ferrite with CuO-rich grain boundary segregation. *J. Alloy. Comp.* **595**, 206 (2014).
  70. R.A. Mondal, B.S. Murty, and V.R.K. Murthy: Origin of magnetocapacitance in chemically homogeneous and inhomogeneous ferrites. *Phys. Chem. Chem. Phys.* **17**, 2432 (2015).
  71. H.I. Yoon, D.K. Lee, H.B. Bae, G.Y. Jo, H.S. Chung, J.G. Kim, S.J. Kang, and S.Y. Chung: Probing dopant segregation in distinct cation sites at perovskite oxide polycrystal interfaces. *Nat. Commun.* **8**, 1417 (2017).
  72. W. Cao, A. Kundu, Z. Yu, M.P. Harmer, and R.P. Vinci: Direct correlations between fracture toughness and grain boundary segregation behavior in ytterbium-doped magnesium aluminate spinel. *Scr. Mater.* **69**, 81 (2013).
  73. P. Zachariasz, J. Kulawik, and P. Gudzek: Preparation and characterization of the microstructure, dielectric and magneto-electric properties of multiferroic Sr<sub>3</sub>CuNb<sub>2</sub>O<sub>9</sub>-CoFe<sub>2</sub>O<sub>4</sub> ceramics. *Mater. Des.* **86**, 627 (2015).
  74. C. Boyle, P. Carvillo, Y. Chen, E.J. Barbero, D. Mcintyre, and X. Song: Grain boundary segregation and thermoelectric performance enhancement of bismuth doped calcium cobaltite. *J. Eur. Ceram. Soc.* **36**, 601 (2016).
  75. T. Nagano, K. Tamahashi, Y. Sasajima, and J. Onuki: Cs corrected STEM observation and atomic modeling of grain boundary impurities of very narrow Cu interconnect. *ECS Electrochem. Lett.* **2**, H23 (2013).
  76. Z. Yu, Q. Wu, J.M. Rickman, H.M. Chan, and M.P. Harmer: Atomic resolution observation of Hf doped alumina grain boundaries. *Scr. Mater.* **68**, 703 (2013).
  77. T. Walther, M. Hopkinson, N. Daneau, A. Recnik, Y. Ohno, K. Inoue, and I. Yonenaga: How to best measure atomic segregation to grain boundaries by analytical transmission electron microscopy. *J. Mater. Sci.* **49**, 3898 (2014).
  78. K. Babinsky, J. Weidow, W. Knabl, A. Lorich, H. Leitner, and S. Primig: Atom probe study of grain boundary segregation in technically pure molybdenum. *Mater. Charact.* **87**, 95 (2014).
  79. M.J.R. Sandim, D. Tytko, A. Kostka, P. Choi, S. Awaji, K. Watanabe, and D. Raabe: Grain boundary segregation in a bronze-route Nb<sub>3</sub>Sn superconducting wire studied by atom probe tomography. *Supercond. Sci. Technol.* **26**, 05508 (2013).

80. Y.J. Li, P. Choi, S. Goto, C. Borchers, D. Raabe, and R. Kirchheim: Atomic scale investigation of redistribution of alloying elements in pearlitic steel wires upon cold-drawing and annealing. *Ultramicroscopy* **132**, 233 (2013).
81. Y.J. Li, D. Ponge, P. Choi, and D. Raabe: Segregation of boron at prior austenite grain boundaries in a quenched martensitic steel studied by atom probe tomography. *Scr. Mater.* **96**, 13 (2015).
82. M. Herbig, D. Raabe, Y.J. Li, P. Choi, S. Zaeferrer, and S. Goto: Atomic scale quantification of grain boundary segregation in nanocrystalline material. *Phys. Rev. Lett.* **112**, 126103 (2013).
83. S. Mandal, K.G. Pradeep, S. Zaeferrer, and D. Raabe: A novel approach to measure grain boundary segregation in bulk polycrystalline materials in dependence of the boundaries' five rotational degrees of freedom. *Scr. Mater.* **81**, 16 (2014).
84. K.N. Solanki, M.A. Tschopp, M.A. Bhatia, and N.R. Rhodes: Atomistic investigation of the role of grain boundary structure on hydrogen segregation and embrittlement in  $\alpha$ -iron. *Metall. Mater. Trans. A* **44**, 1365 (2013).
85. N.R. Rhodes, M.A. Tschopp, and K.N. Solanki: Quantifying the energetics and length scales of carbon segregation to  $\alpha$ -Fe symmetric tilt grain boundaries using atomistic simulations. *Modell. Simul. Mater. Sci. Eng.* **21**, 035009 (2013).
86. C.X. Li, S.H. Dang, L.P. Wang, C.L. Zhang, and P.D. Han: First principles investigation into effects of Cr on segregation of S and Cl at  $\alpha$ -Fe  $\Sigma 5(210)$  grain boundary. *Mater. Res. Innovations* **18**, S41012 (2014).
87. H. Jin, I. Elfimov, and M. Militzer: Study of the interaction of solutes with  $\Sigma 5(013)$  tilt grain boundary in iron using density-functional theory. *J. Appl. Phys.* **115**, 093506 (2014).
88. A.M. Tahir, R. Janisch, and A. Hartmaier: Hydrogen embrittlement of a carbon segregated  $\Sigma 5(310)[001]$  symmetrical tilt grain boundary in  $\alpha$ -Fe. *Mater. Sci. Eng., A* **612**, 462 (2014).
89. S.K. Bhattacharya, M. Kohyama, S. Tanaka, and Y. Shiihara: Si segregation at Fe grain boundaries analyzed by ab initio local energy and local stress. *J. Phys.: Condens. Matter* **26**, 355005 (2014).
90. T. Suzudo and M. Yamaguchi: Simulation of He embrittlement at grain boundaries in bcc transition metals. *J. Nucl. Mater.* **465**, 695 (2015).
91. M.R. Zemła, J.S. Wróbel, T. Wejrzanowski, D. Nguyen-Manh, and K.J. Kurzydłowski: The helium effect at grain boundaries in Fe-Cr alloys? A first-principles study. *Nucl. Instrum. Methods Phys. Res., Sect. B* **393**, 118 (2017).
92. E.L.T. Bentría, I.K. Lefkaier, and B. Bentría: The effect of vanadium impurity on nickel  $\Sigma 5(210)$  grain boundary. *Mater. Sci. Eng., A* **577**, 197 (2013).
93. V.I. Razumovskiy, A.Y. Lozovoi, and I.M. Razumovskii: First-principles-aided design of a new Ni-base superalloy: Influence of transition metal alloying elements on grain boundary and bulk cohesion. *Acta Mater.* **82**, 369 (2015).
94. A.V. Subashiev and H.H. Nee: Hydrogen trapping at divacancies and impurity-vacancy complexes in nickel: First principles study. *J. Nucl. Mater.* **487**, 135 (2017).
95. N.K. Das, T. Shoji, T. Nishizumi, T. Fukuoka, T. Sugawara, R. Sasaki, T. Tatsuki, H. Yuya, K. Ito, K. Tatsumi, S. Ooki, Y. Sueishi, and K. Takada: First-principles calculations of hydrogen interactions with nickel containing a monovacancy and divacancies. *Mater. Res. Express* **4**, 076505 (2017).
96. S. Divi, G. Agrahari, S.R. Kadulkar, S. Kumar, and A. Chatterjee: Improved prediction of heat of mixing and segregation in metallic alloys using tunable mixing rule for embedded atom method. *Modell. Simul. Mater. Sci. Eng.* **25**, 085011 (2017).
97. M. Všianská, H. Vémolová, and M. Šob: Segregation of sp-impurities at grain boundaries and surfaces: Comparison of fcc cobalt and nickel. *Modell. Simul. Mater. Sci. Eng.* **25**, 085004 (2017).
98. M. Rajagopalan, M.A. Bhatia, K.N. Solanki, and M.A. Tschopp: Investigation of atomic-scale energetics on liquid metal embrittlement of aluminum due to gallium. *TMS Ann. Meet.* **2014**, 1069 (2014).
99. X.J. Shen, D. Tanguy, and D. Connétable: Atomistic modelling of hydrogen segregation to the  $\Sigma 9(221)[110]$  symmetric tilt grain boundary in Al. *Philos. Mag.* **94**, 2247 (2014).
100. H. Wang, M. Kohyama, S. Tanaka, and Y. Shiihara: First-principles study of Si and Mg segregation in grain boundaries in Al and Cu: Application of local-energy decomposition. *J. Mater. Sci.* **50**, 6864 (2015).
101. L.E. Karkina, I.N. Karkin, A.R. Kuzetsov, I.K. Razumov, P.A. Korzhavyi, and Y.N. Gornostyrev: Solute-grain boundary interaction and segregation formation in Al: First principles calculations and molecular dynamics modeling. *Comput. Mater. Sci.* **112**, 18 (2016).
102. L. Huber, B. Grabowski, M. Militzer, J. Neugebauer, and J. Rottler: Ab initio modelling of solute segregation energies to a general grain boundary. *Acta Mater.* **132**, 138 (2017).
103. D. Scheiber, R. Pippan, P. Puschnig, A. Ruban, and L. Romaner: Ab initio search for cohesion-enhancing solute elements at grain boundaries in molybdenum and tungsten. *Int. J. Refract. Met. Hard Mater.* **60**, 75 (2016).
104. D. Scheiber, R. Pippan, P. Puschnig, and L. Romaner: Ab-initio search for cohesion-enhancing impurity elements at grain boundaries in molybdenum and tungsten. *Modell. Simul. Mater. Sci. Eng.* **24**, 085009 (2016).
105. N. Chen, L.L. Niu, Y. Zhang, X. Shu, H.B. Zhou, S. Jin, G. Ran, G.H. Lu, and F. Gao: Energetics of vacancy segregation to  $[100]$  symmetric tilt grain boundaries in bcc tungsten. *Sci. Rep.* **6**, 36955 (2014).
106. J. Chai, Y.H. Li, L.L. Niu, S.Y. Qin, H.B. Zhou, J. Shuo, Y. Zhang, and G.H. Lu: First-principles investigation of the energetics of point defects at a grain boundary of tungsten. *Nucl. Instrum. Methods Phys. Res., Sect. B* **393**, 144 (2017).
107. X.X. Wang, L.L. Niu, and S. Wang: Strong trapping and slow diffusion of helium in a tungsten grain boundary. *J. Nucl. Mater.* **487**, 158 (2017).
108. L. Sun, S. Jin, H.B. Zhou, Y. Zhang, and G.Y. Lu: Dissolution and diffusion of hydrogen in a molybdenum grain boundary: A first-principles investigation. *Comput. Mater. Sci.* **102**, 243 (2015).
109. O. Lenchuk, J. Rohrer, and K. Albe: Atomistic modelling of zirconium and silicon segregation at twist and tilt grain boundaries in molybdenum. *J. Mater. Sci.* **51**, 1873 (2016).
110. A. Lindman, E.E. Helgee, B.J. Nyman, and G. Wahnström: Oxygen vacancy segregation in grain boundaries of BaZrO<sub>3</sub> using interatomic potentials. *Solid State Ionics* **230**, 27 (2013).
111. E.E. Helgee, A. Lindman, and G. Wahnström: Origin space charge in grain boundaries of proton conducting BaZrO<sub>3</sub>. *Fuel Cells* **13**, 19 (2013).
112. A. Lindman, E.E. Helgee, and G. Wahnström: Theoretical modeling of defect segregation and space charge formation in the BaZrO<sub>3</sub> (210)[001] tilt grain boundary. *Solid State Ionics* **252**, 121 (2013).
113. J.H. Yang, B.K. Kim, and Y.C. Kim: Calculations of proton conductivity at the  $\Sigma 3(111)[\bar{1}\bar{1}0]$  tilt grain boundary of barium zirconate using density functional theory. *Solid State Ionics* **279**, 60 (2015).
114. J.S. Kim and Y.C. Kim: Proton conduction in nonstoichiometric  $\Sigma 3$  BaZrO<sub>3</sub> (210)[001] tilt grain boundary using density functional theory. *J. Korean Ceram. Soc.* **53**, 301 (2017).



115. A. Lindman, T.S. Bjørheim, and G. Wahnström: Defect segregation to grain boundaries in BaZrO<sub>3</sub> from first principles free energy calculations. *J. Mater. Chem. A* **5**, 13421 (2017).
116. M. Všíanská and M. Šob: The effect of segregated sp-impurities on grain-boundary and surface structure, magnetism and embrittlement in nickel. *Prog. Mater. Sci.* **56**, 817 (2011).
117. P. Lejček and S. Hofmann: Thermodynamics of grain boundary segregation and applications to anisotropy, compensation effect and prediction. *Crit. Rev. Solid State Mater. Sci.* **33**, 133 (2008).
118. P. Lejček, M. Šob, V. Paidar, and V. Vitek: Why calculated energies of grain boundary segregation are unreliable when segregant solubility is low. *Scr. Mater.* **68**, 547 (2013).
119. P. Rez and J.R. Alvarez: Calculation of cohesion and changes in electronic structure due to impurity segregation at boundaries in iron. *Acta Mater.* **47**, 4069 (1999).
120. M. Yuasa and M. Mabuchi: Bond mobility mechanism in grain boundary embrittlement: First-principles tensile tests of Fe with a P-segregated  $\Sigma 3$  grain boundary. *Phys. Rev. B* **82**, 094108 (2010).
121. M. Yuasa and M. Mabuchi: First-principles study on enhanced grain boundary embrittlement of iron by phosphorus segregation. *Mater. Trans.* **52**, 1369 (2011).
122. R. Wu, A.J. Freeman, and G.B. Olson: First principles determination of phosphorus and boron on iron grain boundary cohesion. *Science* **265**, 376 (1994).
123. Y.Q. Fen and C.Y. Wang: Electronic effects of nitrogen and phosphorus on iron grain boundary cohesion. *Comput. Mater. Sci.* **20**, 48 (2001).
124. M. Yamaguchi: First-principles study on the grain boundary embrittlement of metals by solute segregation: Part I. Iron (Fe)-solute (B, C, P, and S) systems. *Metall. Mater. Trans. A* **42**, 319 (2011).
125. M. Yamaguchi: First-principles calculations of the grain-boundary cohesive energy—Embrittling or strengthening effect of solute segregation in a bcc Fe $\Sigma 3(111)$  grain boundary. *J. Japan Inst. Met.* **72**, 657 (2008).
126. M. Rajagopalan, M.A. Tschopp, and K.N. Solanki: Grain boundary segregation of interstitial and substitutional impurity atoms in alpha-iron. *JOM* **66**, 129 (2014).
127. W.S. Ko, J.B. Jeon, C.H. Lee, J.K. Lee, and B.J. Lee: Intergranular embrittlement of iron by phosphorus segregation: An atomistic simulation. *Modell. Simul. Mater. Sci. Eng.* **21**, 025012 (2013).
128. S. Braithwaite and P. Rez: Grain boundary impurities in iron. *Acta Mater.* **53**, 2715 (2005).
129. E. Wachowicz and A. Kiejna: Effect of impurities on structural, cohesive and magnetic properties of grain boundaries in  $\alpha$ -Fe. *Modell. Simul. Mater. Sci. Eng.* **19**, 025001 (2011).
130. M. Všíanská and M. Šob: to be published.
131. W.S. Ko, N.J. Kim, and B.J. Lee: Atomistic modeling of an impurity element and metal-impurity system: pure P and Fe-P system. *J. Phys.: Condens. Matter* **24**, 225002 (2012).
132. P. Lejček, S. Hofmann, and J. Janovec: Prediction of enthalpy and entropy of solute segregation at individual grain boundaries of  $\alpha$ -iron and ferrite steels. *Mater. Sci. Eng., A* **462**, 76 (2007).
133. H. Erhart and H.J. Grabke: Equilibrium segregation of phosphorus at grain boundaries of Fe-P, Fe-C-P, Fe-Cr-P, and Fe-Cr-C-P alloys. *Met. Sci.* **15**, 401 (1981).
134. Y. Zhang, W.Q. Feng, Y.L. Liu, G.H. Lu, and T. Wang: First-principles study of helium effect in a ferromagnetic iron grain boundary: Energetics, site preference and segregation. *Nucl. Instrum. Methods Phys. Res., Sect. B* **267**, 3200 (2009).